BIOCHEMISTRY
including biophysical chemistry & molecular biology

ARTICLE

pubs.acs.org/biochemistry

Determinants of the Heme−CO Vibrational Modes in the H-NOX Family

Rosalie Tran,[†,‡] Emily E. Weinert,[†,‡] Elizabeth M. Boon,[†,∥] Richard A. Mathies,[*,†,‡] and Michael A. Marletta[*,†,‡,§]

[†]Department of Chemistry, [‡]California Institute for Quantitative Biosciences, and [§]Department of Molecular and Cellular Biology, University of California, Berkeley, California 94720, United States

Supporting Information

ABSTRACT: The *H*eme *N*itric oxide/*OX*ygen binding (H-NOX) family of proteins have important functions in gaseous ligand signaling in organisms from bacteria to humans, including nitric oxide (NO) sensing in mammals, and provide a model system for probing ligand selectivity in hemoproteins. A unique vibrational feature that is ubiquitous throughout the H-NOX family is the presence of a high C−O stretching frequency. To investigate the cause of this spectroscopic characteristic, the Fe−CO and C−O stretching frequencies were probed in the H-NOX domain from *Thermoanaerobacter tengcongensis* (*Tt* H-NOX) using resonance Raman (RR) spectroscopy. Four classes of heme pocket mutants were generated to assess the changes in stretching frequency: (i) the distal H-bonding network, (ii) the proximal histidine ligand, (iii) modulation of the heme conformation via Ile-5 and Pro-115, and (iv) the conserved Tyr-Ser-Arg (YxSxR) motif. These mutations revealed important electrostatic interactions that dampen the back-donation of the Fe^{II} d_π electrons into the CO π^* orbitals. The most significant change occurred upon disruption of the H-bonds between the strictly conserved YxSxR motif and the heme propionate groups, producing two dominant CO-bound heme conformations. One conformer was structurally similar to *Tt* H-NOX WT, whereas the other displayed a decrease in ν(C−O) of up to ∼70 cm^{-1} relative to the WT protein, with minimal changes in ν(Fe−CO). Taken together, these results show that the electrostatic interactions in the *Tt* H-NOX binding pocket are primarily responsible for the high ν(C−O) by decreasing the Fe $d_\pi \rightarrow$ CO π^* back-donation and suggest that the dominant mechanism by which this family modulates the Fe^{II}−CO bond likely involves the YxSxR motif.

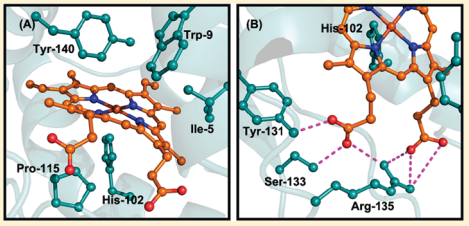

Recently, a novel class of heme proteins, the *H*eme−*N*itric oxide/*OX*ygen binding (H-NOX) domains was identified through sequence similarity to the heme domain of mammalian soluble guanylate cyclase (sGC). sGC is the mammalian receptor for NO and is involved in various functions such as blood vessel dilation. In addition, studies have suggested that H-NOX domains may be gas sensors in a variety of prokaryotes. The H-NOX family of heme proteins has the distinctive property in that some members bind only NO and CO, whereas others can also form a stable complex with O_2, thereby providing an avenue for probing ligand selectivity within heme proteins.[1−3] A unique feature that is shared by all H-NOX domains, and may contribute to ligand binding properties, is an unusually high C−O stretching frequency observed in the heme−CO adducts. This mode, which typically occurs in other heme proteins at vibrational frequencies that are 20−50 cm^{-1} lower than that observed for the H-NOX family, is sensitive to the protein environment surrounding the bound ligand and can provide detailed insight on how the heme binding pocket possibly interacts with other diatomic gases, such as NO or O_2. Despite the availability of NMR and X-ray crystal structures for several of these H-NOX domains,[3−7] the factors that are responsible for the high ν(C−O) and the biochemical implications of this stretching mode remain unclear.

Resonance Raman (RR) spectroscopy is a powerful tool to probe heme protein−ligand interactions in solution, especially with heme−CO adducts because the nature of these interactions can be readily elucidated from the Fe−CO and C−O stretching frequencies since these modes are highly sensitive to the electrostatic field of the distal pocket and the donor properties of the proximal ligand. Extensive density functional theory (DFT) computations and vibrational studies on both heme proteins and synthetic model porphyrins have previously shown that the Fe−CO and C−O vibrational frequencies are negatively correlated due to back-bonding effects; the Fe^{II} d_π electrons are back-donated to the CO π^* orbitals, strengthening the Fe−CO bond while weakening the C−O bond.[8−25] Thus, a key focus in investigating these H-NOX proteins via RR spectroscopy is to better understand the interactions between the exogenous diatomic ligands (e.g., O_2, NO, and CO) and the H-NOX heme-binding pocket using the Fe^{II}−CO adduct as a general model. A deeper appreciation of the complex protein−ligand interactions will not only reveal how the C−O stretching frequency is modulated in these heme domains but may also help determine key components that are responsible for controlling ligand specificity in the H-NOX family.

Received: April 12, 2011
Revised: June 21, 2011
Published: June 29, 2011

In addition to the high ν(C−O) frequency in the H-NOX family, CO is also of interest as it weakly activates sGC upon binding to the heme prosthetic group.[26] The 2−4-fold increase in catalytic activity upon CO binding is significantly lower than the 100−400-fold increase upon NO binding to sGC; however, the activity can be modulated by small molecules such as the benzylindazole derivative, YC-1 [3-(5′-hydroxymethyl-3′-furyl)-1-benzylindazole]. RR investigations have shown changes in the heme conformation and associated CO vibrational modes upon introduction of these small molecules, suggesting that they interact with the heme prosthetic group.[27−34] Furthermore, previous work found that truncation of full length sGC to its heme domain, β1(1−194), resulted in a ∼20 cm^{-1} ν(C−O) downshift to ∼1968 cm^{-1}.[35−38] These results suggest that the protein structure and conformational flexibility also influence the CO stretching frequency.

In this study, RR spectroscopy is used in conjunction with site-directed mutagenesis and isotopic substitution to evaluate how different features within the H-NOX domain from *Thermoanaerobacter tengcongensis* (*Tt* H-NOX) affect the C−O stretching frequency and elucidate the binding site interactions between the ligand-bound heme and the protein environment. The specific H-NOX properties investigated in this work include (i) the presence of H-bonding distal residues in the binding pocket, (ii) the bond strength and steric constraints of the proximal ligand, (iii) heme deformation, and (iv) H-bonding between the conserved Tyr-Ser-Arg (YxSxR) motif and the propionate substituents of the heme (Figure 1). Our RR spectra not only provide insight into these interactions in solution and their influence on the Fe-CO bond in *Tt* H-NOX but also provide a plausible mechanism for signal transduction from the heme to associated signaling components in this broad family of diatomic sensors.

MATERIALS AND METHODS

Protein Expression and Purification. Expression and purification of the his-tagged (-H_6) *Tt* H-NOX domain were performed as previously described.[39] Site-directed mutagenesis was carried out using the QuikChange protocol (Agilent) and verified by sequencing (UC Berkeley sequencing core).

The *Tt* H-NOX H102G mutant was expressed and purified with imidazole (Im) as the proximal ligand using the same methods described for the WT protein, with the following modifications. Imidazole (10 mM) was added to the expression cultures at the time of induction with isopropyl-β-D-1-thiogalactopyranoside (IPTG). In addition, 10 mM imidazole was added to buffer A (50 mM TEA, 20 mM NaCl, 5% glycerol, pH 7.5) during purification to ensure retention of the heme in the *Tt* H-NOX H102G mutant.

Sample Preparation. Purified *Tt* H-NOX-H_6 protein was brought into an anaerobic glovebag and oxidized using 5−10 mM potassium ferricyanide to remove the bound O_2. The ferricyanide was removed using a PD10 desalting column (GE Healthcare) equilibrated with buffer B (50 mM TEA, 50 mM NaCl, pH 7.5). Following oxidation and desalting, the protein was reduced with ∼5−20 mM sodium dithionite that was removed using a PD10 desalting column upon complete reduction of the heme. To make the ^{12}CO (Praxair) and ^{13}CO (^{13}C, 99%; ^{18}O, <2%; Cambridge Isotopes) complexes, gas was added to a sealed Reacti-Vial (Pierce) containing Fe^{II}-unligated protein. Final sample concentrations for the Raman experiments were typically 15−30 μM for the ferrous unligated proteins and ∼35−75 μM for the CO complexes. All UV/vis absorption samples were prepared and measured as previously described.[1,40]

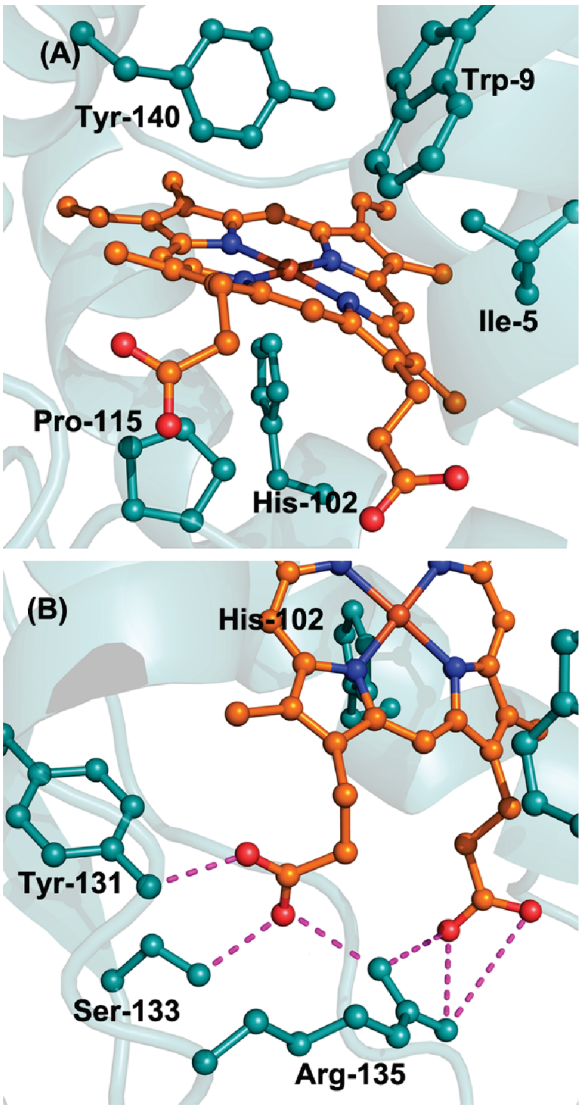

Figure 1. Structure of the heme pocket of *Tt* H-NOX highlighting the locations of important residues (PDB 1U55). (A) Overview of the distal and proximal pockets, showing the hydrogen-bonding network, proximal His-102, and residues associated with heme deformation (Ile-5 and Pro-115). (B) The conserved YxSxR motif of the H-NOX family.

Other exogenous proximal ligands were substituted into the *Tt* H-NOX H102G mutant in addition to imidazole (Im); these included 1-methylimidazole (1-Me-Im), 2-methylimidazole (2-Me-Im), 4(5)-methylimidazole [4(5)-Me-Im], 4(5)-bromoimidazole [4(5)-Br-Im], 4(5)-iodoimidazole [4(5)-I-Im], pyridine (Pyr), and 3-fluoropyridine (3-F-Pyr). To exchange the proximal ligands, the purified *Tt* H-NOX H102G(Im) protein was heated for 1 h at 50 °C with ∼5−10 mM potassium ferricyanide and then desalted with a PD10 column equilibrated with buffer B containing 10 mM of the appropriate proximal ligand. The desalted protein was then heated at 50 °C for an additional 30 min and reduced with ∼5−20 mM sodium dithionite that was removed using a PD10 desalting column

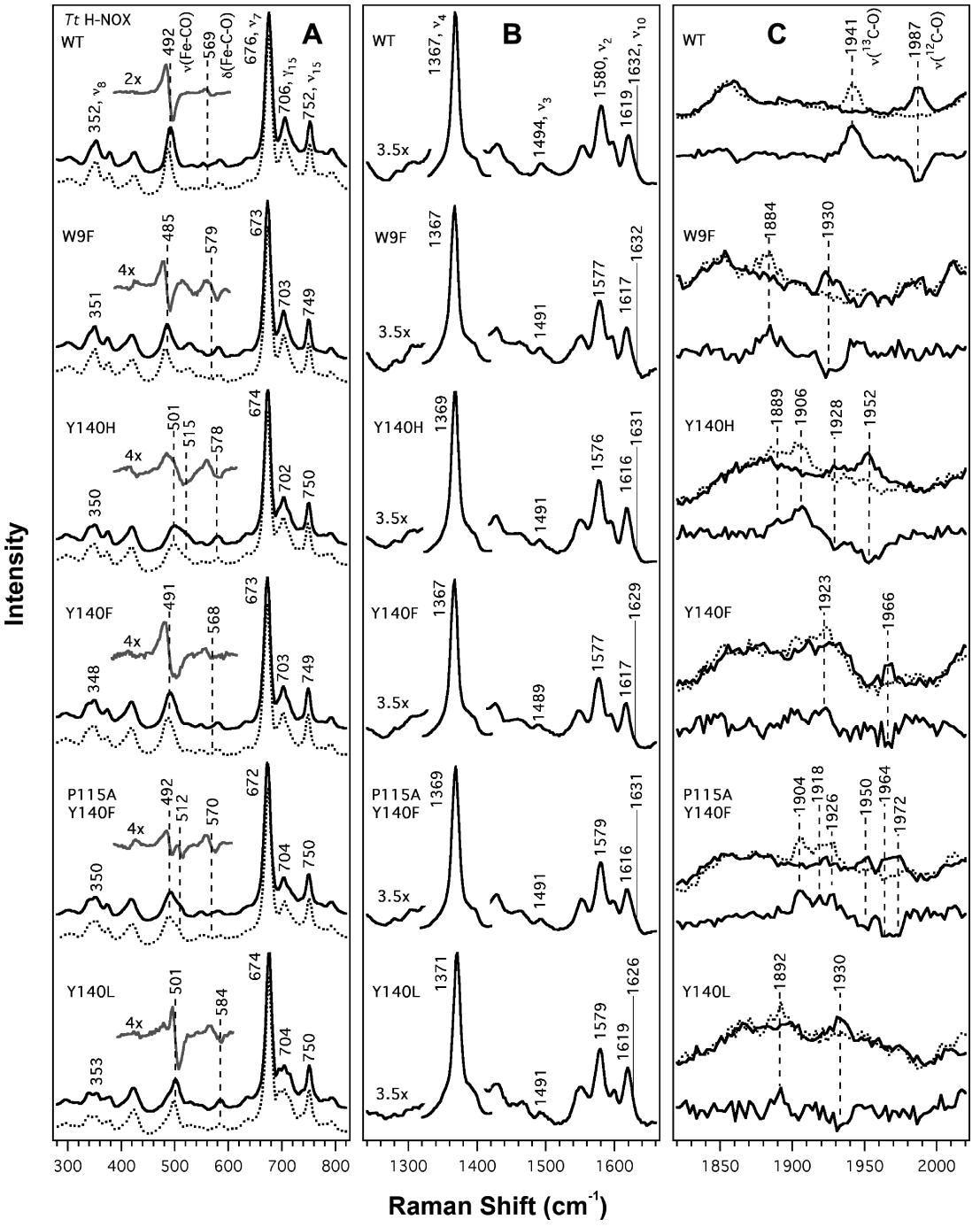

Figure 2. Resonance Raman spectra of the CO complexes of *Tt* H-NOX WT, W9F, Y140H, Y140F, P115A/Y140F, and Y140L. Panel A shows the low-frequency ^{12}CO (solid line), ^{13}CO (dotted line), and magnified (2−4×) difference ($^{13}CO-^{12}CO$) spectra for clarity. Panel B shows the skeletal markers in the high-frequency region; ν_4 has been reduced in size to more clearly display the markers. Panel C displays a magnified view of the CO stretch region, with ^{13}CO (dotted) and ^{12}CO (solid) overlaid, and the difference spectra ($^{13}CO-^{12}CO$) included below. Spectral intensities were normalized to ν_7 and ν_4 for the low- and high-frequency regions, respectively.

upon complete reduction of the heme. This method was sufficient to exchange the imidazole with the alternate proximal ligands. Once the proximal ligand was substituted, generation of the ferrous unligated and CO-bound forms were performed as described above.

Resonance Raman Spectroscopy. All spectra were collected using the 413.1 nm line from a Kr^+ laser (Spectra-Physics model 2025) as previously described.[41] The protein samples were anaerobically loaded into a microspinning Raman sample cell, described previously,[42] in a glovebag to avoid the possibility of O_2 binding. The power at the sample was 2 mW, except for the CO complexes, where the laser power was reduced to ∼250 μW to minimize CO photolysis. Typical data acquisition times were 60−90 min. Electronic absorption spectra were obtained before and after the Raman experiments to verify that no photoinduced degradation occurred. Raman spectra were corrected for wavelength dependence of the spectrometer efficiency with a white lamp, and

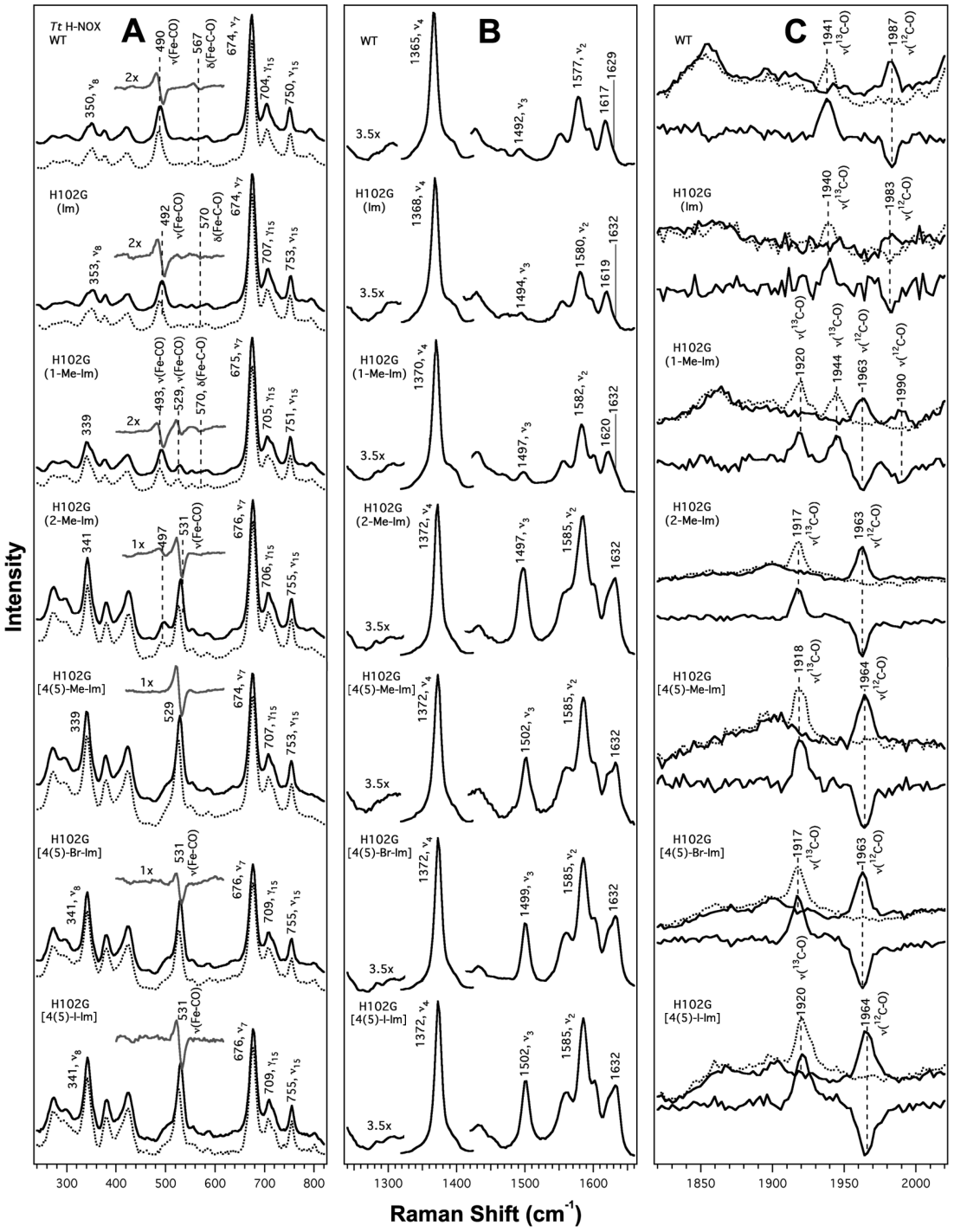

Figure 3. Resonance Raman spectra of the CO complexes of *Tt* H-NOX WT and the *Tt* H102G mutant with 1 mM of the following proximal ligands: imidazole (Im), 1-Me-Im, 2-Me-Im, 4(5)-Me-Im, 4(5)-Br-Im, and 4(5)-I-Im. Panel A shows the low-frequency ^{12}CO (solid line), ^{13}CO (dotted line), and magnified (1−2×) difference ($^{13}CO-^{12}CO$) spectra for clarity. Panel B shows the skeletal markers in the high-frequency region; ν_4 has been reduced in size to more clearly display the markers. Panel C displays a magnified view of the CO stretch region, with ^{13}CO (dotted) and ^{12}CO (solid) overlaid, and the difference spectra ($^{13}CO-^{12}CO$) included below. Spectral intensities were normalized to ν_7 and ν_4 for the low- and high-frequency regions, respectively.

the instrument was calibrated using the Raman frequencies from cyclohexane, CCl_4, and toluene. The reported frequencies are accurate to ±1 cm^{-1}, and the spectral bandpass was set to 8 cm^{-1}. For each Raman spectrum, the raw data were baseline-corrected, and the buffer background signal was subtracted. Spectral analysis was performed using Igor Pro (WaveMetrics). Theoretical isotopic shifts were approximated on the basis of a simple harmonic oscillator model.

RESULTS AND DISCUSSION

To characterize the conformational and electronic changes of the heme chromophore in the *Tt* H-NOX mutants, electronic

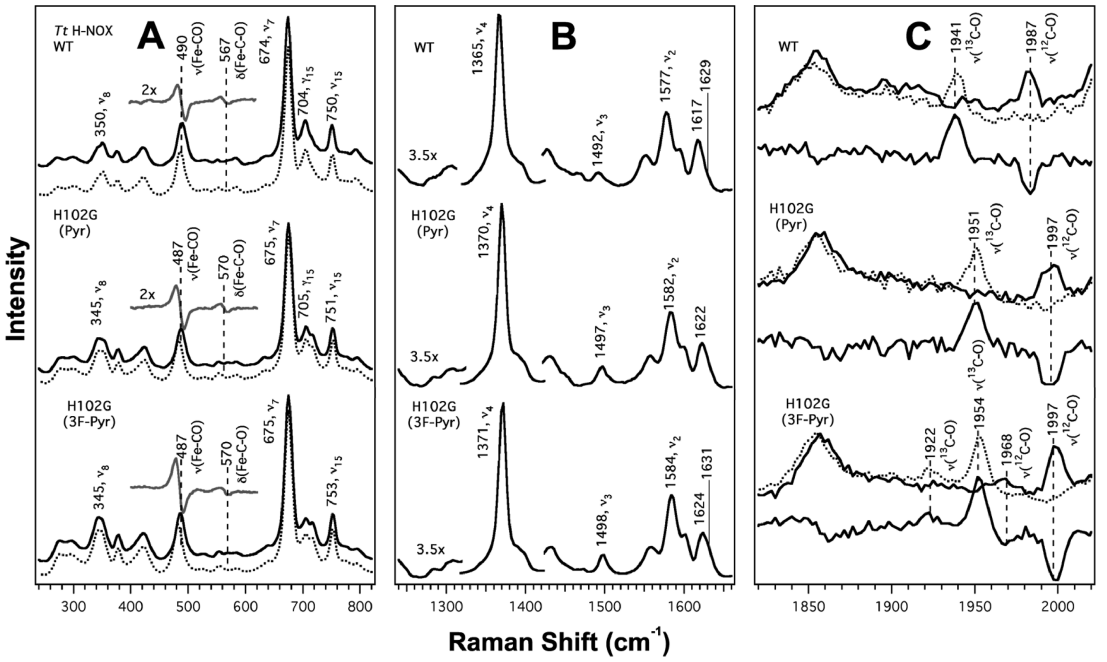

Figure 4. Resonance Raman spectra of the CO complexes of *Tt* H-NOX WT and the *Tt* H102G mutant with 1 mM of the proximal ligands, pyridine (Pyr), and 3-F-Pyr. Panel A shows the low-frequency ^{12}CO (solid line), ^{13}CO (dotted line), and magnified (1−2×) difference (^{13}CO−^{12}CO) spectra for clarity. Panel B shows the skeletal markers in the high-frequency region; ν_4 has been reduced in size to more clearly display the markers. Panel C displays a magnified view of the CO stretch region, with ^{13}CO (dotted) and ^{12}CO (solid) overlaid, and the difference spectra (^{13}CO−^{12}CO) included below. Spectral intensities were normalized to ν_7 and ν_4 for the low- and high-frequency regions, respectively.

absorption and RR measurements on the ferrous unligated and CO-bound forms were carried out (Figures 2−6; Supporting Information Tables S1−S4). The RR spectra of the *Tt* H-NOX CO complexes are organized by mutations made in the heme pocket that involve (i) distal H-bonding residues, (ii) proximal ligand substitution, (iii) heme deformation, and (iv) the YxSxR motif. In addition, the heme skeletal modes, ν(Fe-His), and CO-associated modes are tabulated (Supporting Information Tables S3 and S4) for comparison with other heme proteins.[1,27,35−37,43−46] Through careful analysis of the RR data presented here together with the available NMR and X-ray crystallographic results,[3−7] a more comprehensive understanding of the heme structure and its interactions with the H-NOX protein environment has been developed.

Distal Electrostatic Effects on CO-Bound *Tt* H-NOX. As the distal pocket H-bonding residues have previously been shown to be important determinants of O_2 binding and affinity in the H-NOX family, the effect of distal pocket mutants on the electronics of heme−ligand binding were investigated using the Fe^{II}−CO adducts. Previous studies with other heme proteins reported modulations in the ν(Fe−CO)/ν(C−O) back-bonding correlation upon altering the polar interactions between the CO ligand and distal residues.[9,14,17−23,44] A notable example is the Mb double mutant H64V/V68T, which produced vibrational frequencies of 479 and 1984 cm^{-1} for the Fe−CO and C−O stretching modes, respectively, in comparison to the native Mb protein [ν(Fe−CO) ∼512 cm^{-1}; ν(C−O) ∼1944 cm^{-1}].[20] The decreased back-bonding in this double mutant was thought to result from negative polarity in the distal pocket due to lone electron pairs from the oxygen in Thr-68 being directed at the CO ligand, diminishing back-bonding and increasing the C−O bond order. This negative polarity in the distal pocket forces electron density back to the Fe center and decreases the Fe−C bond order. Similar trends were previously demonstrated in synthesized superstructured iron twin-coronet porphyrin models with naphthalene hydroxyl groups overhanging the bound CO moiety.[47]

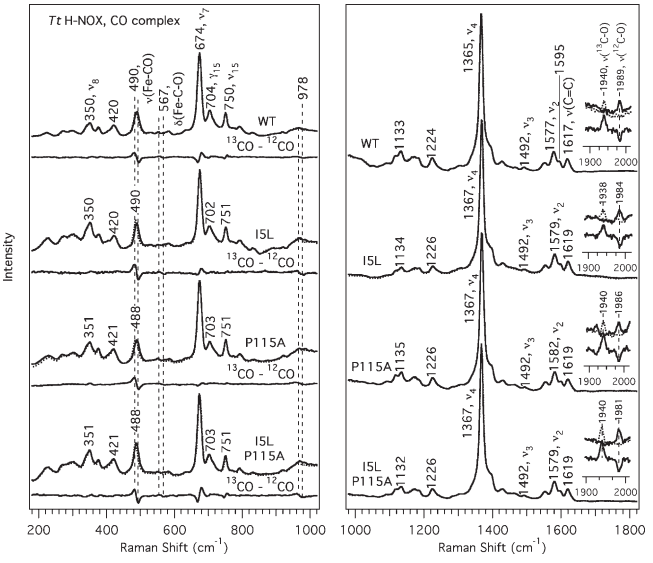

Figure 5. Resonance Raman spectra of the CO complexes of *Tt* H-NOX WT, I5L, P115A, and I5L/P115A. ^{13}CO spectra (dotted line) are overlaid upon the ^{12}CO spectra to indicate the frequency shifts upon isotopic substitution, and the difference (^{13}CO−^{12}CO) spectra are shown below each protein for clarity. Insets show the isotopic shift trends for ν(C−O) in the 1850−2000 cm^{-1} region. Spectral intensities were normalized to ν_7 and ν_4 for the low- and high-frequency regions, respectively.

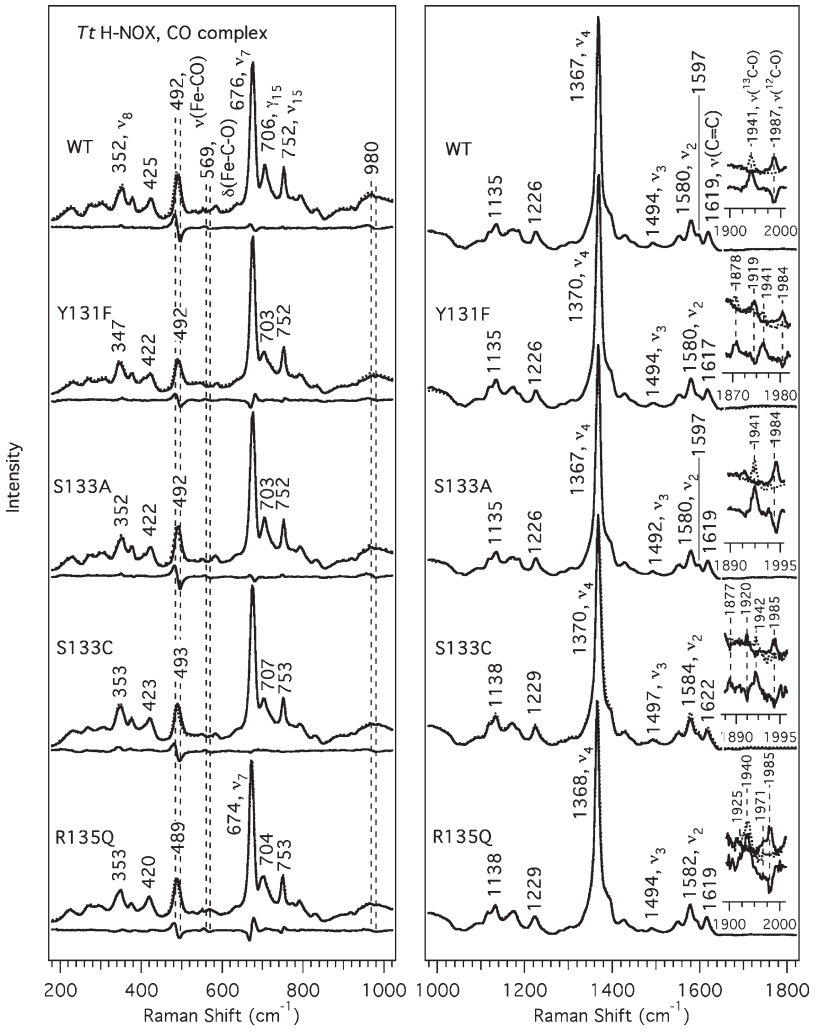

Figure 6. Resonance Raman spectra of the CO complexes of *Tt* H-NOX WT, Y131F, S133A, S133C, and R135Q. ^{13}CO spectra (dotted line) are overlapped over the ^{12}CO spectra to indicate the frequency shifts upon isotopic substitution, and the difference ($^{13}CO-^{12}CO$) spectra are shown below each protein for clarity. Insets show the isotopic shift trends for ν(C−O) in the 1850−2000 cm^{-1} region. Spectral intensities were normalized to ν_7 and ν_4 for the low- and high-frequency regions, respectively.

The *Tt* H-NOX WT protein has a similar CO stretching frequency to that of the Mb H64V/V68T double mutant [*Tt* H-NOX WT, ν(C−O) ∼1987 cm^{-1} vs Mb H64V/V68T, ν(C−O) ∼1984 cm^{-1}]; thus, the *Tt* H-NOX distal pocket may also contain a localized negative polarity with the oxygen from Tyr-140 directly above the CO ligand. Although no crystal structures of the CO-bound *Tt* H-NOX domain are available, previous structural studies from Pellicena et al.,[3] Ma et al.,[6] and Erbil et al.[7] strongly indicate that the CO moiety would bind in a mostly linear geometry in the heme pocket and could directly interact with the two lone pairs of the hydroxyl group of the Tyr-140 distal residue as indicated in the simplified schematic representation of the CO-bound *Tt* H-NOX (Figure 7).

Several previously studied CO-bound myoglobin variants exhibited an increase in the ν(C−O) frequency upon replacement of the distal histidine residue with a nonpolar residue that cannot form H-bonding contacts with the bound CO (Supporting Information Figure S4).[20] This results from the increased electron density around the CO moiety upon removal of the H-bond from the distal His-64 residue, decreasing the effects of back-donation from the Fe^{II} d_π electrons into the CO

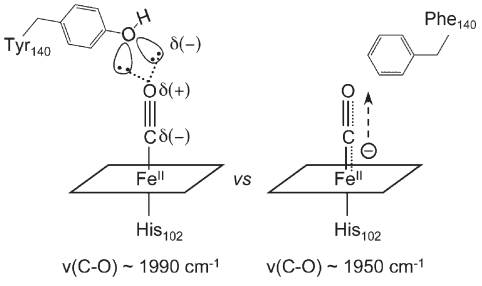

Figure 7. Interaction between Tyr-140 and CO in *Tt* H-NOX. The electron lone pairs from Tyr-140 point toward the CO moiety in *Tt* H-NOX WT. Upon mutation to a hydrophobic residue, the negative polarity introduced by Tyr-140 is abolished so back-donation from the Fe^{II} d_π orbital into the CO π^* orbital increases, weakening the CO bond strength.

π^* orbitals and increasing the CO bond order. In contrast, the RR spectra reported here indicate a decrease in the C−O stretching frequency upon disruption of the distal H-bonding network in *Tt* H-NOX (Figure 2). In particular, both the *Tt* H-NOX Y140F and

Y140L mutants display C−O stretching modes at 1966 and 1930 cm^{-1}, respectively, which are lower in frequency relative to the WT protein [ν(C−O) ~1987 cm^{-1}]. This observation is the opposite of the trends previously observed in Mb[9,14,15,17,19,20] and suggests that Tyr-140 does not form an H-bond with the CO moiety in the native *Tt* H-NOX protein. Furthermore, the previous work on the Mb H64V/V68T double mutant suggests the possibility that the lone electron pairs from the Tyr-140 oxygen point toward the CO moiety in *Tt* H-NOX. Therefore, the negative polarity should be abolished upon substitution of Tyr-140 with a hydrophobic residue, resulting in a decrease in the observed ν(C−O) (Figure 7).

In the *Tt* H-NOX WT protein, Tyr-140 is held in place by a H-bonding network that involves Trp-9 and Asn-74.[3] To investigate the influence of this extended H-bonding network on the C−O stretching frequency, attention was focused on the nearby Trp-9 residue in the distal pocket (Figure 1A). Mutation of Trp-9 to phenylalanine disrupts the H-bonding network, and a significant ~60 cm^{-1} downshift to ~1930 cm^{-1} is observed in ν(C−O). It is plausible that, by removing Trp-9, Tyr-140 is allowed to freely rotate into a H-bonding interaction with the bound CO ligand. The combination of replacing the original oxygen lone pair interaction with a H-bonding one would then produce the observed ~60 cm^{-1} ν(C−O) downshift. Similar to ν(C−O), the Fe−CO stretching mode also decreases to 485 cm^{-1} and broadens relative to the WT protein (Figure 2). The observed broadening of the Fe−CO stretching mode likely reflects the fact that the Tyr-140 residue has more freedom of motion upon disruption of the H-bonding network. The fact that the Fe−CO stretch also displayed a decrease in frequency despite such a large decrease in the C−O stretching frequency strongly suggests that there are other effects counterbalancing the increased back-donation from the Fe^{II} d_π electrons into the CO π^* orbitals. Although competition from the *trans* axial ligand for σ-overlap with the Fe d_z^2 orbital could counterbalance the expected increase in the Fe−CO stretching mode,[20] this seems unlikely since there is no anticipated change to the donor strength of the proximal histidine ligand with the W9F mutation. One possibility is the presence of a modest Fe−CO displacement off the heme *z*-axis plane upon formation of distal H-bonding interactions, which would reduce the π bonding and result in deviations from the back-bonding correlation.[8,21] From DFT studies, Kozlowski et al. found that both the C−O and Fe−CO stretching frequencies decrease as the oxygen atom is displaced from the heme *z*-axis due to orbital misalignment.[8] Thus, it is possible that this modest displacement, in addition to the H-bonding interaction between the CO ligand and distal Tyr-140, may account for the decreased frequencies observed in both ν(Fe−CO) and ν(C−O) for the CO complex in *Tt* H-NOX W9F.

Another unique aspect of the RR spectra was the presence of multiple CO conformers upon mutation of Tyr-140 to histidine, evidenced by two observed ν(C−O) frequencies at 1928 and 1952 cm^{-1} (Figure 2). This is further supported by the broadened Fe−CO stretching mode observed in *Tt* H-NOX Y140H with a peak at 501 cm^{-1} and a shoulder at ~515 cm^{-1}. The presence of multiple conformers in the CO-bound *Tt* H-NOX Y140H mutant may be reflective of a loosely held histidine residue in the distal pocket, resulting in two different transient H-bonding interactions between the CO moiety and the protonated N_{His}. The reduced CO stretching frequencies that are observed would be consistent with an H-bond interaction between these two groups for both conformers. The only other distal pocket variant to display multiple CO conformations was the double mutant, *Tt* H-NOX P115A/Y140F, which displayed broad CO stretching modes at 1950 and 1964−1972 cm^{-1}, in addition to broad Fe−CO stretching modes at 492 and 512 cm^{-1}. We have previously suggested that the single P115A mutation sufficiently disrupts the hinging region of the H-NOX domain, resulting in a more "open" conformation that relaxes the heme.[4,7,41] This increased opening of the distal and proximal regions of the H-NOX domain would certainly provide dynamic disorder within the heme pocket, making accessible protein−ligand contacts more transient. This effect, in combination with the structural rearrangements to accommodate the Y140F mutation, is plausibly responsible for the multiple conformations and peak broadening observed in the P115A/Y140F double mutant.

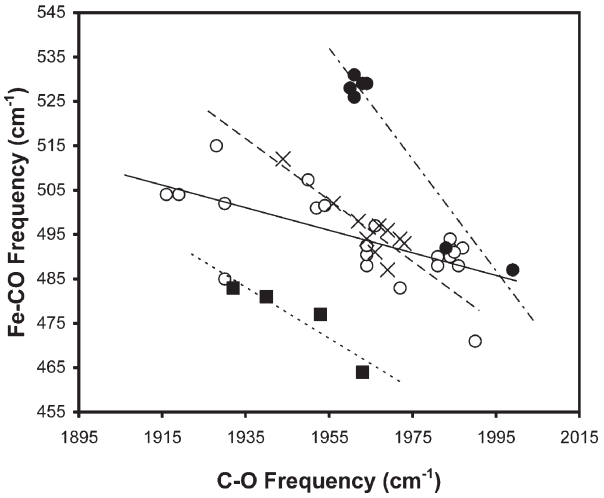

Figure 8. Back-bonding correlation plot between ν(Fe−CO) and ν(C−O) for several H-NOX domains and other heme proteins. The CO-bound heme proteins and the corresponding symbols for the plot are as follows: H-NOX domains (○); *Tt* H-NOX H102G with substituted proximal ligands (●); other histidyl-ligated heme proteins (×); P450s (■).

Although the idea of a localized negative polarity from the hydroxyl group of the Tyr-140 residue in the distal pocket provides a reasonable interpretation for the high ν(C−O) in *Tt* H-NOX and the consequent downshifts in frequency upon distal pocket mutation, it does not extend to the rest of the H-NOX family due to the absence of this residue in the H-NOX domains from facultative aerobes. In fact, structural studies on the H-NOX domains from *Shewanella oneidensis* and *Nostoc sp* indicate a predominantly nonpolar distal pocket lined with mostly hydrophobic residues.[6,7] Thus, other contributing factors (e.g., electrostatic or steric) from the H-NOX heme pocket must also play a role in the unusually high ν(C−O) frequency. These additional factors may provide insight as to how members of the H-NOX family with the same fold are able to exhibit different ligand selectivities.

Modulation via the Proximal Ligand. It is well-known that the axial residue ligand trans to the CO influences the back-bonding between the Fe^{II} and CO. This effect of the axial ligand is readily observed from the back-bonding plot (Figure 8) showing the ν(Fe−CO)/ν(C−O) correlations among heme proteins with different proximal ligands (e.g., imidazole versus thiolate).[11,12,20,21,23,48,49] Vogel et al. also previously showed that

the ligand proximal to the CO displaces the back-bonding plots, altering the slopes and lowering the Fe−CO stretching frequency. Changes in the back-bonding slope depend on the donor strength of the proximal ligand and occur due to the competition between the proximal ligand and CO for σ-orbital overlap with the Fe^{II} d_{z^2} acceptor orbital.[23,24] With the increased electron density on the heme metal due to the proximal ligand, back-donation from Fe^{II} d_π to CO π^* is increased and the C−O bond weakens.

Tt H-NOX WT has a Fe−His stretching frequency of ~217 cm^{-1}, which is indicative of a weak to moderate H-bond to the proximal ligand in comparison to no H-bond [ν(Fe−His) ~200 cm^{-1}] and a strong H-bond [ν(Fe−His) ~240 cm^{-1}].[49] On the basis of the similarity in vibrational frequency, it is possible that the *Tt* H-NOX WT protein contains a Mb-like imidazole H-bond to either a carbonyl group of the protein backbone, a nearby proximal residue, or water. No crystal structures of the Fe^{II}-unligated *Tt* H-NOX exist, so it is uncertain what is forming this moderate H-bond with His-102 in *Tt* H-NOX. However, on the basis of the O_2-bound *Tt* H-NOX crystal structure by Pellicena et al.,[3] the H-bond is plausibly between the N_δ proton of His-102 and the backbone carbonyl of Met-98. The 2.8 Å distance between the N_δ of His-102 and backbone carbonyl oxygen from Met-98 is comparable to the ~2.9 Å distances between the corresponding H-bonding residues in *Sw* Mb, His-93, Ser-92, and Leu-89.[50]

In the H-NOX family, the vibrational frequency of the Fe−His stretching mode ranges from 208 to 224 cm^{-1} (Supporting Information Table S3). Despite these varying Fe−His bond strengths, the observed ν(Fe−CO) and ν(C−O) frequencies remain remarkably similar across the H-NOX family (Supporting Information Table S4). Thus, it does not appear that the strength of the Fe−His bond alone contributes to the unusually high C−O stretching frequency. However, it is important to note here that these observations do not necessarily rule out a functional role of the Fe−His bond within multicomponent signaling mechanisms that involve the H-NOX domain. Previous studies have already shown that ν(Fe−His) increases from 204 to 208 cm^{-1} as sGC is truncated down to the β(1−194) domain;[36−38] thus, additional RR studies on the full-length proteins with their associated signaling components (e.g., histidine kinases, methyl-accepting chemotaxis domains, or diguanylate cyclases) should be completed before such conclusions are made.

To probe the role of the proximal ligand in modulating the ligand binding properties of the H-NOX family, the proximal ligand was systematically exchanged with a series of imidazole derivatives within the same protein scaffold via the *Tt* H-NOX H102G mutant. These imidazole derivatives produced a range of Fe−N_{im} stretching frequencies from 188 to 215 cm^{-1}. Despite similarities in heme skeletal mode frequencies for the 5-coordinated fully reduced *Tt* H-NOX H102G variants, the RR spectra exhibited significant shifts in both the vibrational frequency and intensity for the CO complexes (Figures 3 and 4). Several CO-bound *Tt* H-NOX H102G variants [e.g., 2-Me-Im, 4(5)-Me-Im, 4(5)-Br-Im, and 4(5)-I-Im] displayed a dominant CO conformer with a ν(Fe−CO) at 526−531 cm^{-1} and a ν(C−O) at 1960−1964 cm^{-1} (Figure 3). However, when 1-Me-Im was incorporated as a proximal Fe ligand, an additional conformer appeared in the RR spectra with a ν(Fe-CO) at ~493−497 cm^{-1} and ν(C−O) at ~1984−1990 cm^{-1} (Figure 3). Since the vibrational frequencies for the Fe−CO and C−O stretching modes in *Tt* H-NOX H102G(Im) [ν(Fe−CO) ~492 cm^{-1}, ν(C−O) ~1983 cm^{-1}] are similar to those of the WT protein [ν(Fe−CO) ~490 cm^{-1}, ν(C−O) ~1987 cm^{-1}], it is clear that the substantial shifts observed for the other proximal ligands are directly related to the additional substituents. Interestingly, the *Tt* H-NOX H102G(Pyr) and H102G(3-F-Pyr) proteins exhibited increased ν(C−O) frequencies at 1997 cm^{-1} in comparison to the WT protein [ν(C−O) ~1987 cm^{-1}] despite the significantly reduced ν(Fe−N_{pyr}) frequencies of 203 and 197 cm^{-1} for pyridine and 3-F-pyridine, respectively (Figure 4; Supporting Information Table S4).

There are several possible explanations for these spectral differences between the *Tt* H-NOX H102G proteins and WT (ν(Fe−CO) ~490 cm^{-1}, ν(C−O) ~1987 cm^{-1}), including (i) the changes in the ligand pK_a, (ii) the size, strain, and orientation of the ligand within the proximal pocket, and (iii) the ability to form H-bonds with nearby proximal residues or the protein backbone. From the inverse relationship between the Fe−CO and C−O stretching mode frequencies, it is evident that these modes are coupled. Depending on the change in the net coupling between these two modes, the vibrational frequencies for ν(Fe−CO) and ν(C−O) will shift accordingly. Thus, geometric distortions in either the Fe−N_{im} or Fe−CO bonds are likely to alter this vibrational coupling, modulating the Fe $d_\pi \rightarrow$ CO π^* back-donation and influencing the magnitude of the ν(Fe−CO) and ν(C−O) shifts.

Furthermore, the heme conformation also appears to be affected by the introduction of the H102G mutation. NMR structures of the CO-bound WT H-NOX and homologous H103G mutant from *Shewanella oneidensis* (*So* H-NOX) were solved by Erbil et al.[7] and found notable ensemble differences between the two structures which suggested changes in the van der Waals contacts between the protein and the heme. The majority of these shifts occurred in the secondary structure region flanking the proximal pocket. Erbil et al. also showed that the heme deformation changed between the *So* H-NOX WT and H103G mutant structures, which is consistent with the RR spectra for the CO-bound *Tt* H-NOX WT and H102G variants. The significant changes observed in both frequency and RR intensity for the *Tt* H-NOX H102G mutants with bulkier proximal ligands [e.g., 2-Me-Im, 4(5)-Me-Im, 4(5)-Br-Im, and 4(5)-I-Im] are suggestive of a 5-coordinate CO complex, with a ν(Fe−CO) that is similar to previously reported 5-coordinate CO complexes.[19,20,29,31,51] Notable differences in the RR spectra for these CO complexes with bulkier imidazole derivatives include increased Raman intensities in the 270−430 cm^{-1} range, a 9−11 cm^{-1} downshift in ν_8 from 350 cm^{-1} in the WT protein, and changes in both the RR intensities and frequencies for several heme skeletal markers in the 1365−1635 cm^{-1} region (Figure 3, panels A and B). In the low-frequency region, the increased Raman intensities of the porphyrin substituent and pyrrole deformation modes (e.g., ν_{52}, γ_7, and γ_6) are consistent with a distortion of the heme as the Fe comes out of the porphyrin plane in an alternate 5-coordinate complex. The domed 5-coordinate porphyrin structure would also have longer Fe−N_{pyr} distances, which is supported by the 9−11 cm^{-1} downshift in ν_8 that is observed for the *Tt* H-NOX H102G mutants containing bulkier proximal ligands. In the high-frequency region, the increased frequencies and intensities observed in the heme skeletal markers are also consistent with a smaller macrocycle cavity resulting from a domed, out-of-plane Fe atom. These differences are further corroborated by electronic absorption spectra of the H102G mutants with bulkier imidazole derivatives, which

showed Soret blue shifts of up to 12 nm from the typical ~423−424 nm position (Supporting Information Table S2). Thus, it is possible that changing the proximal ligand from imidazole to derivatives containing substituents forces the heme into an alternate conformation that would elongate the Fe−N_{im} bond distance and form a transient 5-coordinate CO species, causing more pronounced changes in ν(Fe−CO) and ν(C−O) than previously observed with Mb H93G and with other H-NOX domains containing Fe-His bonds of varying strengths.[1,11,12,38,48]

Influence of the Ile-5 and Pro-115 Residues on Heme Conformation in CO Adducts. To further examine the effects of heme deformation on the CO complex, mutations were generated at Ile-5 and Pro-115, which are known to influence the heme conformation of the O_2-bound WT *Tt* H-NOX domain.[3,4,41] Figure 5 shows the RR spectra for the CO complexes of *Tt* H-NOX WT, I5L, P115A, and the double mutant. In the low-frequency region, the Fe−CO stretching mode is detected at 490 cm^{-1} for the I5L mutant and at 488 cm^{-1} for both the P115A and I5L/P115A mutants, in comparison to 490 cm^{-1} for WT. In the high-frequency region, a single C−O stretching mode is detected between 1981 and 1986 cm^{-1} for the three mutants [ν(C−O) ~ 1989 cm^{-1} for WT]. As is the case with the heme skeletal modes, these measured frequencies are also very similar to those of *Tt* H-NOX WT.

Our RR spectra agree with the DFT calculations of Xu et al. in that there is minimal effect of mutating the residues responsible for heme distortion on the Fe−CO and C−O stretching modes in *Tt* H-NOX.[10] Although the Ile-5 and Pro-115 mutations have been shown to slightly alter the Fe-His strength and influence the heme conformation for the O_2 complexes,[41] both the Fe−CO and C−O frequencies remain remarkably similar to the WT protein at ~490 and ~1985 cm^{-1}, respectively. In addition, the skeletal heme modes do not appreciably shift in frequency, nor do the heme deformation modes display changes in RR intensity. Thus, heme distortion does not appear to affect the Fe^{II}−CO or C−O bonds, as the heme−CO adduct retains binding site interactions similar to those of the WT protein.

Importance of the Conserved YxSxR Motif. The YxSxR motif is strictly conserved throughout the H-NOX family[1−3,7] and provides the anchor for the heme cofactor within the pocket. The crystal structure of WT *Tt* H-NOX shows that Tyr-131 and Ser-133 are within H-bonding distance to one of the heme propionates, while Arg-135 makes contacts with both propionate groups (Figure 1B). Recent DFT calculations by Xu et al. indicated that the neutralization of these negatively charged propionate groups on the heme could modulate the ν(Fe−CO)/ν(CO) back-bonding correlations in a manner similar to electron-withdrawing substituents on porphines, which altered the ν(C−O) frequency by up to ~20 cm^{-1}.[10] Thus, to investigate how the H-bonding of these residues with the propionate substituents influenced the CO complex, mutations were generated at Tyr-131, Ser-133, and Arg-135 of *Tt* H-NOX.

Figure 6 shows the RR spectra of the CO complexes for Tt H-NOX WT, Y131F, S133A, S133C, and R135Q. In all of these mutants, two isotope-sensitive bands at ~490 and ~569 cm^{-1} were detected in the low-frequency region, which correspond to ν(Fe−CO) and δ(Fe−C−O), respectively. No significant frequency shifts were observed in these bands, although a slight spectral broadening of the Fe-CO stretching mode was evident for the *Tt* H-NOX Y131F, S133C, and R135Q mutants (Supporting Information Figure S5). The overall similarity in vibrational frequency indicates that the Fe−CO bond energetics between the WT protein and the four mutants are comparable, whereas the slight broadening of the Fe−CO stretching mode would suggest a larger range of fluctuations in the softened distal pocket. In contrast, the RR spectra showed significant changes in the ν(C−O) frequency for these YxSxR mutants in *Tt* H-NOX [i.e., up to ~70 cm^{-1} shift for ν(C−O)], in addition to surprising dynamics within the heme pocket for the Y131F, S133C, and R135Q mutants, which have not been previously reported. These results provide direct evidence for the importance of the YxSxR motif in stabilizing the heme position and orientation in the H-NOX pocket when the protein is in solution (Figure 1B).

Mutation of Tyr-131 to phenylalanine in *Tt* H-NOX results in the presence of two dominant CO conformers (Figure 6). One form exhibits vibrational features similar to the WT protein, with ν(Fe−CO) and ν(C−O) at ~492 and 1984 cm^{-1}, respectively. The second conformer displays a significantly lower ν(C−O) at 1919 cm^{-1}, yet no other isotope-sensitive band was detected in the lower frequency region for the Fe−CO stretching mode. This mutation abolishes one of the H-bonding contacts between the YxSxR motif and a propionate group. Similarly, the S133C and R135Q mutants display two ν(C−O) bands, but only one dominant ν(Fe-CO) band. Whereas S133C disrupts only one H-bonding contact to one propionate group, the R135Q mutation disrupts H-bonding interactions with both propionate groups. The presence of two CO stretching frequencies, one of which is very similar to the WT protein, may result from a fluctuating swivel motion of the heme prosthetic group upon destabilization of the coordinating H-bonding residues. It is plausible that the heme interchanges between a conformation that retains similar protein−ligand contacts as *Tt* H-NOX WT and another conformation with a very strong H-bond to the CO ligand based on the significantly reduced ν(C−O) frequency of ~1919−1920 cm^{-1}. The source of this strong H-bond could be a water molecule that enters the distal pocket upon mutation due to increased accessibility, although another possibility is that the fluctuating heme motion alters the interaction between Tyr-140 and the CO moiety into one that is H-bonding. The lack of a more appreciable shift in the Fe−CO stretching mode, despite such a large change in the C−O stretching frequency, indicates that there are likely two counterbalancing processes that influence the Fe−CO bond strength. DFT calculations have shown that the transition moment essentially lies along the vector formed by the Fe−C bond, so C−O stretching vibrations induce electrons to travel throughout the π-system.[8,20,52,53] Thus, it is not unreasonable to consider a redistribution of the heme π-conjugation system upon disruption of the neutralizing H-bonds between the propionate groups and the YxSxR motif, which could affect the Fe−CO bond strength.

In contrast, only a single CO conformation is observed in the *Tt* H-NOX S133A mutant with similar Fe−CO and C−O stretching frequencies to those of the WT protein. Ser-133 is sandwiched between Tyr-131 and Arg-135 in the YxSxR motif and is only within H-bonding distance of one of the propionate groups. It is possible that the propionate groups still retained electrostatic interactions with the other two residues; thus, the heme remains in its tightly held position within the H-NOX pocket as in the WT protein. This interpretation is further supported by the spectral similarities between the CO complexes of *Tt* H-NOX WT and S133A in both the vibrational frequencies of the skeletal modes and the relative intensities of the low-frequency out-of-plane modes (i.e., γ_{15} ~706 cm^{-1}). In contrast,

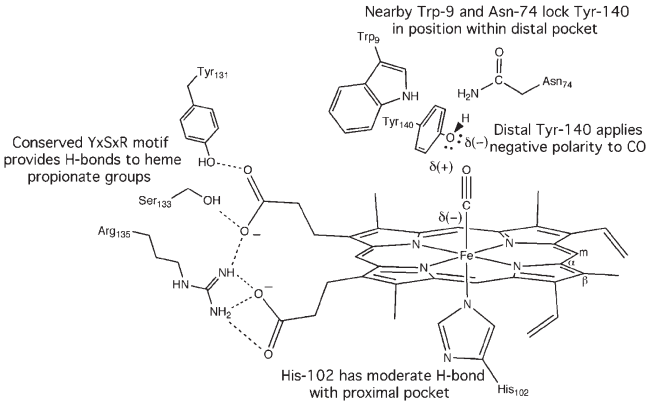

Figure 9. Schematic representation of the heme pocket of *Tt* H-NOX. The different components of the *Tt* H-NOX binding site that can influence the Fe^{II} $d_\pi \rightarrow$ CO π^* back-donation are shown in this diagram: (i) the H-bonding network composed of Trp-9, Asn-74, and Tyr-140 affects the polarity of the distal pocket where CO is bound, (ii) modulation of the axial trans ligand strength can influence how the proximal ligand competes with CO for σ-orbital overlap with Fe, and (iii) H-bonding interactions between the conserved YxSxR motif and heme propionate groups can withdraw electron density from the heme.

the *Tt* H-NOX Y131F, S133C, and R135Q mutants all exhibit small shoulder bands [e.g., $\delta(C_\beta$-vinyl) and $\delta(C_\beta$-$CH_3)$] or slightly decreased RR intensity with broad shoulder peaks (i.e., γ_{15} ~703−707 cm^{-1}) in comparison to the WT protein (Supporting Information Figures S5−S7); this is indicative of alternate heme conformations and/or interactions within the protein pocket.

Modulation of the CO Bond in sGC and the H-NOX Family. It is clear from the RR studies on *Tt* H-NOX and its mutants that a number of factors can influence and likely contribute to the ν(Fe−CO) and ν(C−O) frequencies in heme proteins (Figure 9). Within the H-NOX family, the YxSxR motif is conserved throughout this class of heme proteins and clearly plays an important role in retaining the position of the heme molecule within the protein pocket, as is evident from the RR spectra presented here. Disruption of the tightly held H-bonds between these residues and the heme propionate groups results in altered protein−heme and protein−ligand interactions that can modulate the properties of the H-NOX domain. Not only would electron density from the H-bonds between the YxSxR motif and the propionate groups be redistributed to the heme π-conjugated macrocycle upon neutralizing the negative charges of the porphyrin substituents, but the increased electron density at the metal center would also increase the Fe^{II} $d_\pi \rightarrow$ CO π^* donation. The subsequent heme swiveling motion within the binding site of these YxSxR mutants would also introduce the H-NOX domain to alternate interactions that are different from the WT protein, such as an H-bonding interaction between the CO ligand and distal Tyr-140 residue in *Tt* H-NOX, which can further modulate the Fe $d_\pi \rightarrow$ CO π^* back-donation. It is well-known that electron-donating and -withdrawing groups, whether from porphyrin substituents or nearby polar residues, influence the extent of back-bonding in heme proteins.[8,9,11,12,14−21,23,24,48,53,54] As the back-bonding increases, the Fe−CO stretching frequency rises and the C−O stretching frequency falls. Thus, the YxSxR motif is a critical feature throughout the H-NOX family, not only for the maintenance of both proximal and distal contacts with the heme−CO adduct but for its electrostatic interactions with the porphyrin propionate substituent groups that also influence the ν(C−O) frequency.

Previous RR studies on sGC and the truncated β1 heme domain showed the presence of two CO conformers based on the detection of two Fe−CO stretching frequencies at ~478 and ~487−496 cm^{-1}.[27−30,33,36−38] The majority of these results only reported one stretching frequency for ν(C−O); this discrepancy is likely due to the weak intensity inherent to the C−O stretching mode in RR spectra and the difficulty in obtaining large quantities of full length sGC. Still, an interesting aspect of these prior investigations was that the heme conformer population would shift in favor of one conformation [ν(Fe−CO) ~492 cm^{-1}] over the other [ν(Fe−CO) ~474 cm^{-1}] upon addition of the benzylindazole derivative, YC-1 [3-(5′-hydroxylmethyl-3′-furyl)-1-benzylindazole]. Although much is still unknown about how this small molecule causes the 6-coordinate CO-bound sGC to mimic the fully activated 5-coordinate NO-bound enzyme, it may involve the electrostatic interactions between the conserved YxSxR motif and the propionate side chains of the heme.

Our RR results with the YxSxR mutants of *Tt* H-NOX show remarkable vibrational shifts that are indicative of significant changes in the binding site interactions; thus, these residues may also play an important role in modulating the activation of CO-bound sGC by altering the heme conformation from inactive to active. In addition, our observation that electrostatic changes within the conserved YxSxR motif are coupled to changes in ligand binding and coordination at the Fe center could suggest a much broader role for this motif in the transmission of signal from the heme in the H-NOX domain to associated signaling components, such as the methyl-accepting chemotaxis proteins or histidine kinases. It is clear that there is interplay between ligand binding and the electrostatic interactions of the motif with the heme propionate groups. Since these residues are strictly conserved throughout the H-NOX family, it is plausible that the YxSxR motif may also be important for signal transduction involving H-NOX domains upon binding NO or O_2.

■ ASSOCIATED CONTENT

Supporting Information. Tabulated summaries of the electronic absorption characterization of the Fe^{II}-unligated (Table S1) and CO-bound (Table S2) *Tt* H-NOX; observed vibrational frequencies for the 5-coordinate, Fe^{II}-unligated (Table S3) and CO-bound (Table S4) H-NOX proteins; charts showing correlation trends for ν(Fe−N_{im}), ν(Fe−CO), and ν(C−O) in CO-bound *Tt* H-NOX for distal pocket H-bonding mutants (Figure S1), H102G mutant with alternate proximal ligands (Figure S2), YxSxR mutants (Figure S3), and CO-bound myoglobin with distal mutants (Figure S4) provided for clarity; expanded views of different frequency regions of the resonance Raman spectra for the CO-bound YxSxR motif mutants (Figures S5−S7). This material is available free of charge via the Internet at http://pubs.acs.org.

■ AUTHOR INFORMATION

Corresponding Author

*E-mail ramathies@berkeley.edu, phone 510-642-4192, fax 510-642-3599 (R.A.M.); e-mail marletta@berkeley.edu, phone 510-666-2763, fax 510-666-2765 (M.A.M.).

Present Addresses

[||]Department of Chemistry, Stony Brook University, Stony Brook, NY 11794.

Funding Sources

This work was supported in part by NIH Grant GM070671 (M.A.M.) and the Mathies Royalty Fund.

■ ACKNOWLEDGMENT

We thank Dr. Hans K. Carlson for his help with preparing some of the protein samples for RR measurements, members of the Mathies and Marletta laboratories for discussions, and Patrick Visperas for preliminary characterization of the YxSxR *Tt* H-NOX mutants. We also thank Dr. Mohammed Ibrahim for providing helpful feedback on the RR spectra.

■ ABBREVIATIONS

H-NOX, *H*eme−*N*itric oxide/*OX*ygen binding domain; RR, resonance Raman; *Tt*, *Thermoanaerobacter tengcongensis*; YxSxR, tyrosine-serine-arginine motif; NO, nitric oxide; CO, carbon monoxide; TEA, triethanolamine; DFT, density functional theory.

■ REFERENCES

(1) Karow, D. S., Pan, D., Tran, R., Pellicena, P., Presley, A., Mathies, R. A., and Marletta, M. A. (2004) Spectroscopic characterization of the soluble guanylate cyclase-like heme domains from *Vibrio cholerae* and *Thermoanaerobacter tengcongensis*. *Biochemistry 43*, 10203–10211.

(2) Boon, E. M., and Marletta, M. A. (2005) Ligand specificity of H-NOX domains: from sGC to bacterial NO sensors. *J. Inorg. Biochem. 99*, 892–902.

(3) Pellicena, P., Karow, D. S., Boon, E. M., Marletta, M. A., and Kuriyan, J. (2004) Crystal structure of an oxygen-binding heme domain related to soluble guanylate cyclases. *Proc. Natl. Acad. Sci. U.S.A. 101*, 12854–12859.

(4) Olea, C., Boon, E. M., Pellicena, P., Kuriyan, J., and Marletta, M. A. (2008) Probing the Function of Heme Distortion in the H-NOX Family. *ACS Chem. Biol. 3*, 703–710.

(5) Nioche, P., Berka, V., Vipond, J., Minton, N., Tsai, A. L., and Raman, C. S. (2004) Femtomolar sensitivity of a NO sensor from *Clostridium botulinum*. *Science 306*, 1550–1553.

(6) Ma, X. L., Sayed, N., Beuve, A., and van den Akker, F. (2007) NO and CO differentially activate soluble guanylyl cyclase via a heme pivot-bend mechanism. *EMBO J. 26*, 578–588.

(7) Erbil, W. K., Price, M. S., Wemmer, D. E., and Marletta, M. A. (2009) A structural basis for H-NOX signaling in Shewanella oneidensis by trapping a histidine kinase inhibitory conformation. *Proc. Natl. Acad. Sci. U.S.A. 106*, 19753–19760.

(8) Kozlowski, P. M., Vogel, K. M., Zgierski, M. Z., and Spiro, T. G. (2001) Steric contributions to CO binding in heme proteins: a density functional analysis of FeCO vibrations and deformability. *J. Porphyrins Phthalocyanines 5*, 312–322.

(9) Decatur, S. M., and Boxer, S. G. (1995) A Test of the Role of Electrostatic Interactions in Determining the Co Stretch Frequency in Carbonmonoxymyoglobin. *Biochem. Biophys. Res. Commun. 212*, 159–164.

(10) Xu, C. L., Ibrahim, M., and Spiro, T. G. (2008) DFT analysis of axial and equatorial effects on Heme-CO vibrational modes: Applications to CooA and H-NOX heme sensor proteins. *Biochemistry 47*, 2379–2387.

(11) Decatur, S. M., Belcher, K. L., Rickert, P. K., Franzen, S., and Boxer, S. G. (1999) Hydrogen bonding modulates binding of exogenous ligands in a myoglobin proximal cavity mutant. *Biochemistry 38*, 11086–11092.

(12) Decatur, S. M., DePillis, G. D., and Boxer, S. G. (1996) Modulation of protein function by exogenous ligands in protein cavities: CO binding to a myoglobin cavity mutant containing unnatural proximal ligands. *Biochemistry 35*, 3925–3932.

(13) Kerr, E. A., Mackin, H. C., and Yu, N. T. (1983) Resonance Raman Studies of Carbon-Monoxide Binding to Iron Picket Fence Porphyrin with Unhindered and Hindered Axial Bases - an Inverse Relationship between Binding-Affinity and the Strength of Iron Carbon Bond. *Biochemistry 22*, 4373–4379.

(14) Kushkuley, B., and Stavrov, S. S. (1996) Theoretical study of the distal-side steric and electrostatic effects on the vibrational characteristics of the FeCO unit of the carbonylheme proteins and their models. *Biophys. J. 70*, 1214–1229.

(15) Li, T. S., Quillin, M. L., Phillips, G. N., and Olson, J. S. (1994) Structural Determinants of the Stretching Frequency of Co Bound to Myoglobin. *Biochemistry 33*, 1433–1446.

(16) Li, X. Y., and Spiro, T. G. (1988) Is Bound Co Linear or Bent in Heme-Proteins - Evidence from Resonance Raman and Infrared Spectroscopic Data. *J. Am. Chem. Soc. 110*, 6024–6033.

(17) Phillips, G. N., Teodoro, M. L., Li, T. S., Smith, B., and Olson, J. S. (1999) Bound CO is a molecular probe of electrostatic potential in the distal pocket of myoglobin. *J. Phys. Chem. B 103*, 8817–8829.

(18) Ramsden, J., and Spiro, T. G. (1989) Resonance Raman Evidence That Distal Histidine Protonation Removes the Steric Hindrance to Upright Binding of Carbon-Monoxide by Myoglobin. *Biochemistry 28*, 3125–3128.

(19) Ray, G. B., Li, X. Y., Ibers, J. A., Sessler, J. L., and Spiro, T. G. (1994) How Far Can Proteins Bend the Feco Unit - Distal Polar and Steric Effects in Heme-Proteins and Models. *J. Am. Chem. Soc. 116*, 162–176.

(20) Spiro, T. G., and Wasbotten, I. H. (2005) CO as a vibrational probe of heme protein active sites. *J. Inorg. Biochem. 99*, 34–44.

(21) Spiro, T. G., Zgierski, M. Z., and Kozlowski, P. M. (2001) Stereoelectronic factors in CO, NO and O-2 binding to heme from vibrational spectroscopy and DFT analysis. *Coord. Chem. Rev. 219*, 923–936.

(22) Tsubaki, M., Srivastava, R. B., and Yu, N. T. (1982) Resonance Raman Investigation of Carbon-Monoxide Bonding in (Carbon Monoxy) Hemoglobin and (Carbon Monoxy) Myoglobin - Detection of Fe-Co Stretching and Fe-C-O Bending Vibrations and Influence of the Quaternary Structure Change. *Biochemistry 21*, 1132–1140.

(23) Vogel, K. M., Kozlowski, P. M., Zgierski, M. Z., and Spiro, T. G. (1999) Determinants of the FeXO (X = C, N, O) vibrational frequencies in heme adducts from experiment and density functional theory. *J. Am. Chem. Soc. 121*, 9915–9921.

(24) Vogel, K. M., Kozlowski, P. M., Zgierski, M. Z., and Spiro, T. G. (2000) Role of the axial ligand in heme-CO backbonding; DFT analysis of vibrational data. *Inorg. Chim. Acta 297*, 11–17.

(25) Yu, N. T., Kerr, E. A., Ward, B., and Chang, C. K. (1983) Resonance Raman Detection of Fe-Co Stretching and Fe-C-O Bending Vibrations in Sterically Hindered Carbonmonoxy Strapped Hemes - a Structural Probe of Fe-C-O Distortion. *Biochemistry 22*, 4534–4540.

(26) Stone, J. R., and Marletta, M. A. (1994) Soluble Guanylate-Cyclase from Bovine Lung - Activation with Nitric-Oxide and Carbon-Monoxide and Spectral Characterization of the Ferrous and Ferric States. *Biochemistry 33*, 5636–5640.

(27) Denninger, J. W., Schelvis, J. P. M., Brandish, P. E., Zhao, Y., Babcock, G. T., and Marletta, M. A. (2000) Interaction of soluble guanylate cyclase with YC-1: Kinetic and resonance Raman studies. *Biochemistry 39*, 4191–4198.

(28) Li, Z. Q., Pal, B., Takenaka, S., Tsuyama, S., and Kitagawa, T. (2005) Resonance Raman evidence for the presence of two heme pocket conformations with varied activities in CO-bound bovine soluble guanylate cyclase and their conversion. *Biochemistry 44*, 939–946.

(29) Makino, R., Obayashi, E., Homma, N., Shiro, Y., and Hori, H. (2003) YC-1 facilitates release of the proximal his residue in the NO and CO complexes of soluble guanylate cyclase. *J. Biol. Chem. 278*, 11130–11137.

(30) Pal, B., Li, Z. Q., Ohta, T., Takenaka, S., Tsuyama, S., and Kitagawa, T. (2004) Resonance Raman study on synergistic activation of soluble guanylate cyclase by imidazole, YC-1 and GTP. *J. Inorg. Biochem. 98*, 824–832.

(31) Ibrahim, M., Derbyshire, E. R., Marletta, M. A., and Spiro, T. G. (2010) Probing Soluble Guanylate Cyclase Activation by CO and YC-1 Using Resonance Raman Spectroscopy. *Biochemistry 49*, 3815–3823.

(32) Martin, E., Czarnecki, K., Jayaraman, V., Murad, F., and Kincaid, J. (2005) Resonance Raman and infrared spectroscopic studies of high-

output forms of human soluble guanylyl cyclase. *J. Am. Chem. Soc. 127*, 4625–4631.

(33) Pal, B., Tanaka, K., Takenaka, S., and Kitagawa, T. (2010) Resonance Raman spectroscopic investigation of structural changes of CO-heme in soluble guanylate cyclase generated by effectors and substrate. *J. Raman Spectrosc. 41*, 1178–1184.

(34) Pal, B., and Kitagawa, T. (2010) Binding of YC-1/BAY 41−2272 to soluble guanylate cyclase: A new perspective to the mechanism of activation. *Biochem. Biophys. Res. Commun. 397*, 375–379.

(35) Deinum, G., Stone, J. R., Babcock, G. T., and Marletta, M. A. (1996) Binding of nitric oxide and carbon monoxide to soluble guanylate cyclase as observed with resonance Raman spectroscopy. *Biochemistry 35*, 1540–1547.

(36) Schelvis, J. P. M., Zhao, Y., Marletta, M. A., and Babcock, G. T. (1998) Resonance Raman characterization of the heme domain of soluble guanylate cyclase. *Biochemistry 37*, 16289–16297.

(37) Zhao, Y., Schelvis, J. P. M., Babcock, G. T., and Marletta, M. A. (1998) Identification of histidine 105 in the beta 1 subunit of soluble guanylate cyclase as the heme proximal ligand. *Biochemistry 37*, 4502–4509.

(38) Karow, D. S., Pan, D. H., Davis, J. H., Behrends, S., Mathies, R. A., and Marletta, M. A. (2005) Characterization of functional heme domains from soluble guanylate cyclase. *Biochemistry 44*, 16266–16274.

(39) Weinert, E. E., Plate, L., Whited, C. A., Olea, C., and Marletta, M. A. (2010) Determinants of Ligand Affinity and Heme Reactivity in H-NOX Domains. *Angew. Chem., Int. Ed. 49*, 720–723.

(40) Boon, E. M., Davis, J. H., Tran, R., Karow, D. S., Huang, S. H., Pan, D., Miazgowicz, M. M., Mathies, R. A., and Marletta, M. A. (2006) Nitric oxide binding to prokaryotic homologs of the soluble guanylate cyclase β1 H-NOX domain. *J. Biol. Chem. 281*, 21892–21902.

(41) Tran, R., Boon, E. M., Marletta, M. A., and Mathies, R. A. (2009) Resonance Raman Spectra of an O_2-Binding H-NOX Domain Reveal Heme Relaxation upon Mutation. *Biochemistry 48*, 8568–8577.

(42) Kim, M., Mathies, R. A., Hoff, W. D., and Hellingwerf, K. J. (1995) Resonance Raman Evidence That the Thioester-Linked 4-Hydroxycinnamyl Chromophore of Photoactive Yellow Protein Is Deprotonated. *Biochemistry 34*, 12669–12672.

(43) Hu, S. Z., Smith, K. M., and Spiro, T. G. (1996) Assignment of protoheme Resonance Raman spectrum by heme labeling in myoglobin. *J. Am. Chem. Soc. 118*, 12638–12646.

(44) Tomita, T., Gonzalez, G., Chang, A. L., Ikeda-Saito, M., and Gilles-Gonzalez, M. A. (2002) A comparative resonance Raman analysis of heme-binding PAS domains: heme iron coordination structures of the *Bj*FixL, *Ax*PDEA1, *Ec*Dos, and *Mt*Dos proteins. *Biochemistry 41*, 4819–4826.

(45) Andrew, C. R., Green, E. L., Lawson, D. M., and Eady, R. R. (2001) Resonance Raman studies of cytochrome c′ support the binding of NO and CO to opposite sides of the heme: Implications for ligand discrimination in heme-based sensors. *Biochemistry 40*, 4115–4122.

(46) Aono, S., Kato, T., Matsuki, M., Nakajima, H., Ohta, T., Uchida, T., and Kitagawa, T. (2002) Resonance Raman and ligand binding studies of the oxygen-sensing signal transducer protein HemAT from Bacillus subtilis. *J. Biol. Chem. 277*, 13528–13538.

(47) Tani, F., Matsu-ura, M., Ariyama, K., Setoyama, T., Shimada, T., Kobayashi, S., Hayashi, T., Matsuo, T., Hisaeda, Y., and Naruta, Y. (2003) Iron twin-coronet porphyrins as models of myoglobin and hemoglobin: Amphibious electrostatic effects of overhanging hydroxyl groups for successful CO/O_2 discrimination. *Chem.—Eur. J. 9*, 862–870.

(48) Franzen, S., Boxer, S. G., Dyer, R. B., and Woodruff, W. H. (2000) Resonance Raman studies of heme axial ligation in H93G myoglobin. *J. Phys. Chem. B 104*, 10359–10367.

(49) Kitagawa, T. (1988) The Heme Protein Structure and the Iron-Histidine Stretching Mode, in *Biological Applications of Raman Spectroscopy: Resonance Raman Spectra of Heme and Metalloproteins* (Spiro, T. G., Ed.), pp 97−131, John Wiley & Sons, New York.

(50) Vojtechovsky, J., Chu, K., Berendzen, J., Sweet, R. M., and Schlichting, I. (1999) Crystal structures of myoglobin-ligand complexes at near-atomic resolution. *Biophys. J. 77*, 2153–2174.

(51) Yu, N. T., and Kerr, E. A. (1988) Vibrational Modes of Coordinated CO, CN^-, O_2, and NO, in *Biological Applications of Raman Spectroscopy: Resonance Raman Spectra of Heme and Metalloproteins* (Spiro, T. G., Ed.), pp 39−95, John Wiley & Sons, New York.

(52) Spiro, T. G., and Kozlowski, P. M. (1998) Discordant results on FeCO deformability in heme proteins reconciled by density functional theory. *J. Am. Chem. Soc. 120*, 4524–4525.

(53) Spiro, T. G., and Kozlowski, P. M. (2001) Is the CO adduct of myoglobin bent, and does it matter? *Acc. Chem. Res. 34*, 137–144.

(54) Springer, B. A., Sligar, S. G., Olson, J. S., and Phillips, G. N. (1994) Mechanisms of Ligand Recognition in Myoglobin. *Chem. Rev. 94*, 699–714.